

Geophysical Research Letters

RESEARCH LETTER

10.1002/2016GL069820

Key Points:

- The 2015 Wolf volcano (Galápagos) eruption studied using both Sentinel-1A and ALOS-2 satellite radar data
- Coercruption deformation explained with two magma reservoirs at 1 km and 5 km depths below sea level that may be hydraulically connected
- Observed ground deformation may have been influenced by ring fault activity

Correspondence to:

W. Xu,
wenbin.xu@kaust.edu.sa

Citation:

Xu, W., S. Jónsson, J. Ruch, and Y. Aoki (2016), The 2015 Wolf volcano (Galápagos) eruption studied using Sentinel-1 and ALOS-2 data, *Geophys. Res. Lett.*, 43, doi:10.1002/2016GL069820.

Received 31 MAY 2016

Accepted 25 AUG 2016

Accepted article online 31 AUG 2016

The 2015 Wolf volcano (Galápagos) eruption studied using Sentinel-1 and ALOS-2 data

Wenbin Xu^{1,2,3}, Sigurjón Jónsson¹, Joël Ruch¹, and Yosuke Aoki⁴

¹Physical Science and Engineering Division, King Abdullah University of Science and Technology, Thuwal, Saudi Arabia,

²Department of Earth and Planetary Sciences, University of California, Berkeley, California, USA, ³Now at Department of Land Surveying and Geoinformatics, Hong Kong Polytechnic University, Kowloon, Hong Kong, ⁴Earthquake Research Institute, University of Tokyo, Tokyo, Japan

Abstract An energetic eruption started on 25 May 2015 from a circumferential fissure at the summit of Wolf volcano on Isabela Island, western Galápagos. Further eruptive activity within the Wolf caldera followed in mid-June 2015. As no geodetic observations of earlier eruptions at Wolf exist, this eruption provides an opportunity to study the volcano's magmatic plumbing system for the first time. Here we use interferometric synthetic aperture radar (InSAR) data from both the Sentinel-1A and ALOS-2 satellites to map and analyze the surface deformation at four time periods during the activity. These data allow us to identify the two eruption phases and reveal strong coercruption subsidence within the Wolf caldera that is superimposed on a larger volcano-wide subsidence signal. Modeling of the surface displacements shows that two shallow magma reservoirs located under Wolf at ~1 km and ~5 km below sea level explain the subsidence and that these reservoirs appear to be hydraulically connected. We also suggest that the transition from the circumferential to the intracaldera eruption may have involved ring fault activity.

1. Introduction

The Galápagos Archipelago consists of 13 major volcanic islands that are located 1000 km west of Ecuador in the eastern Pacific Ocean. All of the volcanoes in the western Galápagos have an "inverted soup bowl" shape and they possess large calderas [McBirney and Williams, 1969]. Many volcanic eruptions in the western Galápagos have been reported in the historical record [Simkin and Howard, 1970], and geodetic observations from satellites show that all the western Galápagos volcanoes (except Ecuador volcano) have been actively deforming in the last two decades [Amelung *et al.*, 2000; Baker, 2012].

Several recent studies based on geodetic data (GPS and interferometric synthetic aperture radar (InSAR)) have provided important insights into the magma plumbing systems of the volcanoes in the western Galápagos. Some of the volcanoes (Fernandina, Cerro Azul, and Wolf) show evidence of alternating eruptive activity between radial and circumferential dikes [Chadwick and Dieterich, 1995; Bagnardi *et al.*, 2013]. For example, Fernandina had eruptions in 1995 and 2009 fed by radial dikes on the southwest flank [Jónsson *et al.*, 1999; Bagnardi and Amelung, 2012], while an eruption in 2005 came from circumferential fissures near the southern rim of the caldera [Chadwick *et al.*, 2011]. In addition, geodetic data suggest that the magma plumbing system of Fernandina consists of at least two magma reservoirs at different depths [Chadwick *et al.*, 2011; Bagnardi *et al.*, 2013]. The deeper source has been estimated to be at ~5 km below sea level (bsl), causing edifice-wide ground deformation, while the shallow source at ~1 km bsl feeds the flank and summit eruptions and deforms only the summit region.

Wolf volcano is located at the northern end of Isabela Island and has a ~700 m deep caldera that is roughly 6 by 5 km in size (Figure 1). The current shape of the caldera probably resulted from multiple collapses, indicated by several old terraces and caldera-filling lavas that have been cut by the modern caldera [Geist *et al.*, 2005]. At least 10 eruptions are known to have occurred at Wolf since 1797 [Siebert *et al.*, 2010]. Most of this eruptive activity occurred on the southeastern and eastern flanks of the volcano and produced either circumferential eruptive fissures near the caldera's rim or radial fissures on the volcano's flank. In some cases, eruptions took place within the caldera [Chadwick and Howard, 1991]. Prior to 2015, the most recent eruption at Wolf was in 1982. It started from a radial fissure on the eastern flank of the volcano and then switched to an intracaldera vent, with fountains spewing lava more than 700 m in height [Schatz and Schatz, 1983]. Long-term InSAR observations of Wolf showed that the caldera's floor steadily inflated at a rate of 3 cm/yr between 1997 and 2009, resulting in a total uplift of ~50 cm [Baker, 2012].

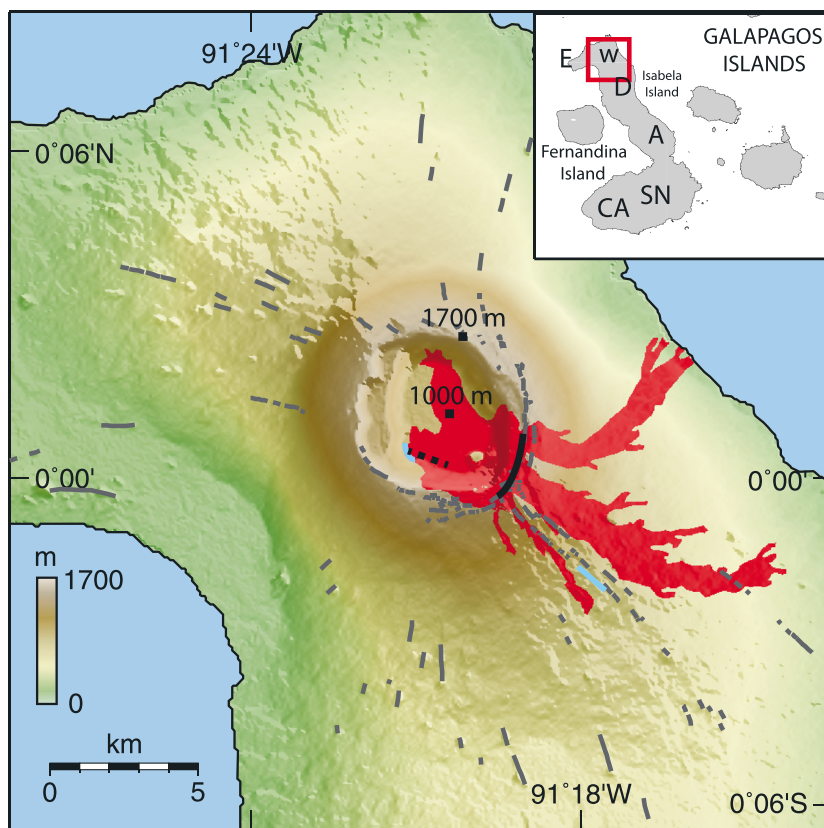


Figure 1. Shaded relief map of Wolf volcano with the 2015 lava flows shown in red. The circumferential eruptive fissure near the southeastern rim of the caldera is marked with a black line, while the inferred dike location within the caldera is shown with a dashed black line. Gray lines represent some older mapped eruptive fissures. Cyan lines show the possible fissure locations of the 1982 eruption. The inset shows the Galápagos islands. E = Ecuador, W = Wolf, D = Darwin, A = Alcedo, SN = Sierra Negra, and CA = Cerro Azul volcanoes.

The 2015 eruption started on 25 May with a circumferential fissure opening near the southeastern rim of the caldera, sending lava down the eastern and southeastern flanks, reaching the sea on 28 May [Global Volcanism Program, 2015]. The eruption started energetically but only lasted eight days and ended on 2 June [Bernard et al., 2015]. Several days later, new eruptive activity was detected within Wolf's caldera. Field observations made by guides and personnel of the Galápagos National Park, overflights, satellite images, and thermal alerts suggest that this intracaldera activity likely began on 11 June (B. Bernard, personal communication, 2016). A Landsat 8 image from 19 June shows fresh lava flows within the caldera moving toward the northern wall. The intracaldera eruption lasted about 1 month and ended on 11 July 2015 [Bernard et al., 2015].

As no geodetic measurements of the 1982 eruption or earlier eruptions at Wolf exist, the 2015 eruption provides a new opportunity to study the volcano's shallow magma plumbing system and to compare it to that of the other volcanoes in the Galápagos. In this paper, we use InSAR observations of the co-eruptive surface deformation and estimate model parameters of sources responsible for the observed changes. We further analyze and discuss the temporal evolution of the ground deformation related to the two eruption locations.

2. InSAR Data Processing

The European Space Agency's (ESA) Sentinel-1A satellite and the Japanese Aerospace Exploration Agency's (JAXA) ALOS-2 satellite acquired SAR data of Wolf volcano both before and during the 2015 eruption. The Sentinel-1A data were collected in the Terrain Observation by Progressive Scan (TOPS) mode, which is similar to a standard Scan-SAR mode, except that the azimuth antenna beam is electronically swept forward in each subswath. This azimuth antenna sweeping causes strong Doppler centroid variations and introduces steep

azimuth phase ramps across TOPS interferograms [Grandin *et al.*, 2015]. Very accurate coregistration in the azimuth direction between master and slave images is required to generate interferograms from TOPS data. To achieve this, we first used the standard intensity cross correlation, which has accuracy of $\sim 1/32$ pixel, for the image coregistration and then we applied a spectral diversity method (which can reach accuracy of $\sim 1/1000$ pixel) in areas where bursts overlap [González *et al.*, 2015]. After the coregistration, we formed interferograms and used the 3 arc second Shuttle Radar Topography Mission (SRTM) digital elevation model for topographic corrections [Farr *et al.*, 2007]. The interferograms were then multilooked and filtered before phase unwrapping with a minimum cost flow method [Chen and Zebker, 2001].

We generated three consecutive interferograms from four Sentinel-1A images acquired at 12 day intervals between 6 May and 23 June 2015, spanning different periods of the Wolf eruption. In addition to these interferograms, we also made one interferogram from a pair of ALOS-2 ScanSAR data spanning the time between 22 May and 3 July 2015, i.e., during most of the eruptive activity. The Sentinel-1A radar operates in C band (5.6 cm wavelength) and these data are more prone to decorrelation and unwrapping errors than are L band ALOS-2 data (23.6 cm wavelength). We therefore used the ALOS-2 interferogram to validate the Sentinel-1A unwrapping, particularly in the area near and within the caldera.

3. InSAR Observations

The four interferograms span different parts of the eruptive activity at Wolf. The first two Sentinel-1A interferograms cover the circumferential fissure eruption near the caldera's rim and the period of inactivity between the two eruptions; the third Sentinel-1A interferogram spans the first third of the later intracaldera eruption, and the ALOS-2 interferogram covers almost the entire eruptive activity. The strongest deformation in the interferograms is found at the center of the caldera's floor and near the circumferential fissure (Figure 2).

3.1. The 6 to 30 May 2015 Interferogram

The interferogram from 6 to 30 May 2015 covers the start of the circumferential fissure eruption on 25 May and its first 5 days (Figure 2a). The observed ground deformation is complex and can be separated into three main signals: (1) a broad volcano-wide zone of negative line-of-sight (LOS) displacement of 10 cm (we define a LOS range increase as negative), i.e., subsidence extending well beyond the caldera; (2) a concentrated fringe pattern limited to the caldera's floor showing strong subsidence of about 40 cm; and (3) positive LOS displacement (15 cm) associated with the circumferential dike opening near the southeastern rim of the caldera (Figure 2a). In addition, this interferogram shows that new lava flowed in three main branches down the southeastern and eastern flanks, causing loss of interferometric coherence. The low coherence on the western flank, on the other hand, is due mostly to dense vegetation.

3.2. The 30 May to 11 June 2015 Interferogram

The interferogram from 30 May to 11 June 2015 covers the last 3 days of the circumferential fissure eruption and the 9 day period of inactivity leading up to the intracaldera eruption. No clear volcano-wide deflation is visible in this interferogram, although atmospheric artifacts make it challenging to verify this (Figure 2d). The strongest deformation in this interferogram is seen near the eruptive fissure, showing localized positive displacement of ~ 12 cm near the southeastern rim of the caldera and subsidence of ~ 5 cm inside the caldera. Postemplacement subsidence of the new lava flows is also clearly visible on the southeastern flank. The northernmost lava flow is still active during this time interval, causing loss of coherence.

3.3. The 11 to 23 June 2015 Interferogram

The third Sentinel-1A interferogram from 11 to 23 June 2015 covers the start of the intracaldera activity (11 June) near the southern wall of the caldera. This activity does not appear to have caused any obvious local ground deformation (Figure 2g). Volcano-wide deflation is seen again in this interferogram, although the fringe pattern is slightly offset to the east compared with what is seen in the first Sentinel-1A interferogram. The maximum observed displacement in this interferogram is subsidence of about 24 cm on the caldera's floor where the new intracaldera lava flow does not cause loss of coherence. Postemplacement subsidence of the northernmost lava flow on the eastern flank is also visible in this interferogram.

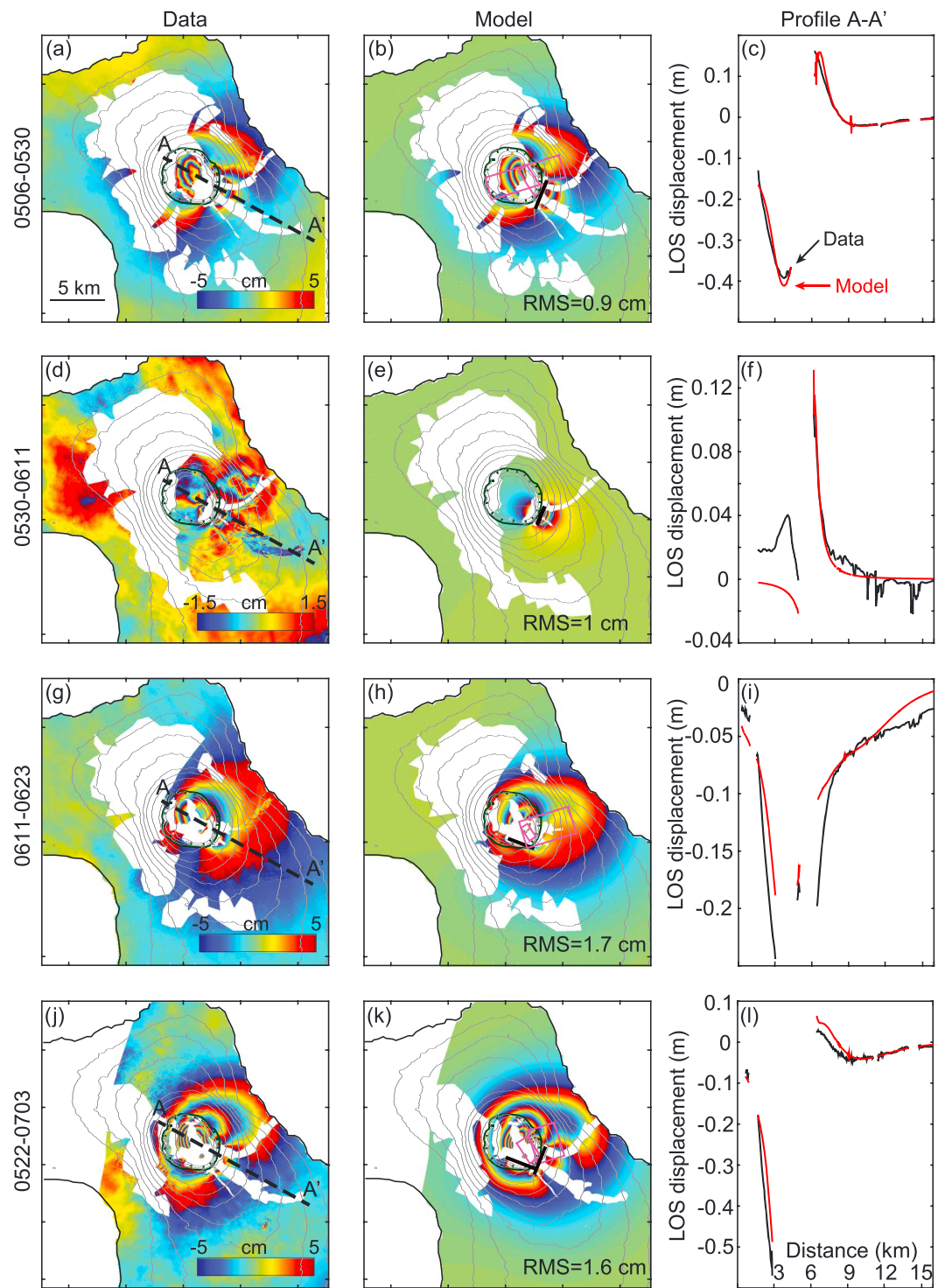


Figure 2. Coeruptive InSAR data of the 2015 Wolf eruption in comparison with model predictions. (a, d, g, and j) The four unwrapped and then rewrapped interferograms used in this study. The scale is the same for all panels; one fringe corresponds to 10 cm line-of-sight (LOS) displacement, except in the second row from top where it is 3 cm. (b, e, h, and k) Model predictions from the optimal models with surface projections of the estimated source planes (black thick lines indicate modeled dikes and purple rectangles the modeled sills). (c, f, i, and l) Observed (black) and modeled (red) displacements along profiles A-A'. The map contour interval is 200 m and the caldera's rim is marked by a ticked line.

3.4. The 22 May to 3 July 2015 Interferogram

The ALOS-2 interferogram from 22 May to 3 July 2015 covers both the circumferential fissure eruption and the majority of the intracaldera activity (Figure 2j), showing strong subsidence of ~60 cm on the caldera's floor, superimposed on the broader volcano-wide subsidence of about 20 cm. These data also indicate that the total subaerial area of the new lava flow is ~25 km², measured from the extent of decorrelated areas in the caldera and on the southeastern flank of the volcano.

4. Estimation of Source Parameters

The InSAR data suggest that at least four sources of deformation were active in Wolf's shallow magmatic system during the 2015 eruption activity. These were a shallow source causing the subsidence within the caldera, a deeper source responsible for the volcano-wide deformation and two dikes feeding the two eruptive fissures. We started to model these sources by using rectangular dislocations [Okada, 1985] with uniform openings or closings with a Poisson's ratio of $\nu=0.25$. To account for the effects of topography in the modeling, we used the topographically corrected modeling (TCM) approach developed by *Williams and Wadge* [2000]. TCM uses a reference elevation for a zero-order modeling solution and then applies first-order corrective terms according to the characteristic slope. It considers the topographical effects in three dimensions and is therefore better than the simpler varying-depth modeling and the reference elevation modeling methods [*Williams and Wadge*, 1998; *Cayol and Cornet*, 1998]. We subsampled our data points using the quadtree method [*Jónsson et al.*, 2002] and weighted the data according to their variance. We then sought model parameters that minimized the weighted root-mean-square misfit between the data and the model's predictions. We estimated the best fitting model parameters by using a Monte Carlo-type simulated annealing algorithm [*Cervelli et al.*, 2001], followed by a gradient-based method.

Since we only have data from descending orbits, we put some initial constraints on the source parameters in the nonlinear estimation. We set the sills to be horizontal, representing the top of the magma reservoirs, and only estimated their depths, horizontal dimensions, and uniform closure values. We tested both point source [*Mogi*, 1958] and ellipsoidal source [*Yang et al.*, 1988] models, but they could not predict deformation patterns that fit the data well. We set the two eruptive dikes to be vertical, fixed their location and strike to match orientations of eruptive fissures, which follow the overall caldera morphology (Figure 1), and solved for the dike dimensions and openings. As multiple sources are active in most of the interferograms, we followed the following three steps: (1) we first estimated the parameters of the circumferential dike; (2) we next fixed the circumferential dike's source parameters and estimated the deep source by masking out the deformation inside the caldera; and (3) we finally estimated the parameters for the shallow sill source and the intracaldera dike.

The best fitting model for the interferogram spanning the start of the eruption includes a deep sill 5.2 km bsl that deflates by 1.1 m (volume decrease of 0.0154 km³). This sill is about 7 km long and 2 km wide, oriented NE-SW (Figure 2b). We estimated the depth of the shallower sill to be 1.3 km bsl with 0.6 m of deflation (volume decrease of 0.0017 km³). It is roughly 2.8 km long and 1 km wide, oriented NW-SE. We found the centers of both sills to be slightly to the east of the center of the caldera. In addition, we estimated the length of the circumferential dike to be 2.5 km with an opening of 0.4 m (Table 1). In the following 12 day period (30 May to 11 June), the optimal model parameters of the dike are smaller (dike length of 1.6 km and opening of 0.1 m), indicating that most of the opening of the dike occurred before 30 May (Figure 2e). In the last Sentinel-1A interferogram (11 June to 23 June), the best fitting model of the deep sill places it around 5 km bsl and sizes it as 4.8 km long and 2.6 km wide. In this model, the shallow sill is 1.2 km bsl (Figure 2h). These sill depths are similar to the best fitting depths found in the first interferogram and again they are centered slightly to the east of the center of the caldera. The deep sill exhibits a volume decrease of 0.015 km³ and the shallow sill a volume decrease of 0.0009 km³. The intracaldera eruptive dike was found to be 2.2 km long with an opening of 0.2 m, while no deformation was seen at the eruptive fissure near the caldera's rim. Overall, the model (for 11 June to 23 June) captures the observed LOS displacement reasonably well. The ALOS interferogram spans the first 6 weeks of the eruption (22 May 2015 to 3 July 2015) and includes deformation from all four sources. The deep sill in the ALOS interferogram is ~5 km bsl, closing by 2.5 m (volume decrease of 0.0215 km³); the shallow sill is 1.3 km bsl, closing by 1 m (volume decrease of 0.0028 km³); the circumferential dike opens 0.5 m and the intracaldera dike opens 0.2 m. The model parameters from the independent ALOS data are in a good agreement with the model parameters that fit the Sentinel-1A data.

Table 1. Information About the Estimated Source Parameters

	Length (km)	Width (km)	Depth (km)	Longitude (deg)	Latitude (deg)	Strike (deg) ^a	Dip (deg) ^a	Opening (m)	Volume Change (km ³)
Source I: Deep Sill									
5/6-5/30	7	2	5.2	-91.33	0.017	253	0	-1.1	-0.0154
5/30-6/11	-	-	-	-	-	-	-	-	-
6/11-6/23	4.8	2.6	5	-91.31	0.01	253	0	-1.2	-0.0150
5/22-7/3	3.3	2.6	5	-91.31	0.017	253	0	-2.5	-0.0215
Source II: Shallow Sill									
5/6-5/30	2.8	1	1.3	-91.326	0.016	147	0	-0.6	-0.0017
5/30-6/11	-	-	-	-	-	-	-	-	-
6/11-6/23	1.5	0.7	1.2	-91.328	0.006	147	0	-0.9	-0.0009
5/22-7/3	2.3	1.2	1.3	-91.33	0.01	147	0	-1	-0.0028
Source III: Dike at the Caldera Rim									
5/6-5/30	2.5	0.5	0 ^a	-91.319 ^a	0.004 ^a	22	90	0.4	0.0005
5/30-6/11	1.6	0.2	0 ^a	-91.319 ^a	0.004 ^a	22	90	0.1	0.0000
6/11-6/23	-	-	- ^a	-91.319 ^a	0.004 ^a	-	-	-	-
5/22-7/3	2.5	0.8	0 ^a	-91.319 ^a	0.004 ^a	22	90	0.5	0.0010
Source IV: Dike within the Caldera									
5/6-5/30	-	-	- ^a	-91.3363 ^a	0.001 ^a	-	-	-	-
5/30-6/11	-	-	- ^a	-91.3363 ^a	0.001 ^a	-	-	-	-
6/11-6/23	2.2	0.7	0 ^a	-91.3363 ^a	0.001 ^a	111	90	0.2	0.0003
5/22-7/3	2.8	0.7	0 ^a	-91.3363 ^a	0.001 ^a	111	90	0.2	0.0004

^aParameters were fixed.

5. Discussion and Conclusions

Our analysis of the spatially and temporally varying ground deformation of Wolf volcano during the 2015 eruption suggests that two shallow magma reservoirs exist at different depths beneath the caldera. A decrease in volume in the shallower reservoir likely caused the observed subsidence that was confined within the caldera, while a volume decrease in the deeper reservoir caused the volcano-wide deformation. By modeling four interferograms separately, we consistently estimated the depths of the two magma reservoirs at ~1 km and ~5 km bsl. Our results also suggest that they are hydraulically connected, as we found concurrent pressure decrease in both during the summit and intracaldera eruptions. We also found that the deep reservoir experienced an order of magnitude greater volume decrease than that in the shallow one during the eruptions. This difference could possibly be due to different magma compressibilities with more exsolved volatiles in the shallow reservoir leading to lower density and compressibility [Rivalta and Segall, 2008]. The difference in volume change could also mean that the deeper reservoir is significantly larger in size than the shallow one, given the pressure drop in the hydraulically connected plumbing system.

An earlier InSAR study, based on data from an intereruption inflation phase, concluded that a shallow reservoir is located under Wolf volcano at ~1 km bsl [Amelung et al., 2000], but it did not report evidence for a

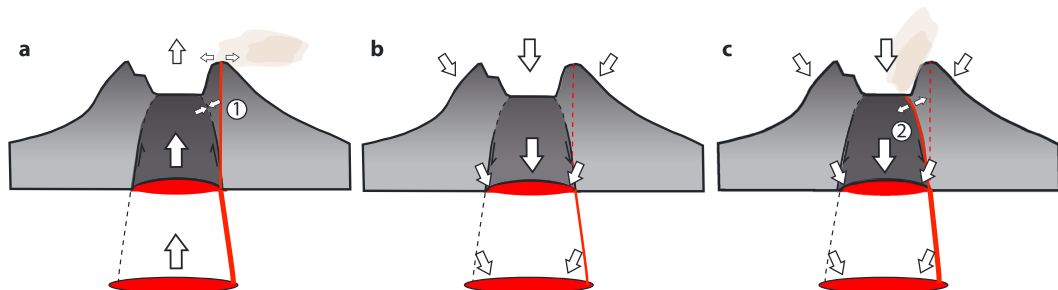


Figure 3. Schematic cross section (NW-SE) across Wolf volcano showing the inferred magma systems and an outward dipping ring fault. (a) The eruption started on 25 May 2015 near the southeastern rim of Wolf's caldera (dike 1), following a steady inflation of the caldera's floor observed from 1997 to 2010 [Baker, 2012]. The magma probably rose through the preferential pathway on the outer caldera rim where extension is expected to maximize after a period of uplift. (b) The emission of lava induced depressurization of the reservoir, partly reactivating the inner outward dipping ring fault. (c) This could have allowed magma to propagate initially along the outward dipping ring fault and erupt within the caldera (dike 2). The figure is not to scale.

deeper reservoir. Analysis and interpretation of petrological and geochemistry data suggest that magmas ascend through a gabbroic mush before stalling in a shallow sill at ~1 km depth bsl at Wolf [Geist *et al.*, 2005], which agrees with our modeled depth of the shallower reservoir. Similar to our results for Wolf, two hydraulically connected magma reservoirs under Fernandina and Cerro Azul volcanoes have been suggested from geodetic and petrological data [Naumann *et al.*, 2002; Chadwick *et al.*, 2011; Bagnardi and Amelung, 2012; Geist *et al.*, 2014]. Interestingly, these two volcanoes have similar morphology to Wolf with deep calderas, asymmetric circumferential fissure zones on top of the caldera rims, and radial fissures on the flanks. Darwin, Alcedo, and Sierra Negra volcanoes have similar features but their calderas are less than 200 m deep, possibly reflecting different stages of collapse cycles.

The eruptions of Wolf volcano in 1982 and 2015 were similar in terms of eruption style with the first intrusion located outside the caldera and then another vent becoming active within the caldera. About 50 cm of uplift were observed at Wolf volcano from 1997 to 2009, while only a few centimeters of uplift occurred in 1992–1997. In both cases the uplift was limited to the caldera floor [Baker, 2012]. The strongest co-eruption subsidence signal was also within the caldera. This sharply bounded uplift deformation within the caldera could possibly be due to buried outward dipping ring fault activity [Bathke *et al.*, 2015; Gudmundsson *et al.*, 2016] (Figure 3a). Long-term uplift (i.e., reservoir inflation) in the presence of caldera topography would cause tension along the caldera rim and on its flanks [Acocella *et al.*, 2015], whereas compression would occur at the caldera's floor and on the shallow part of the ring fault (Figure 3a). In this scenario, intrusions preferentially develop into circumferential dikes (Figure 3a), as observed at Wolf during the early phase of the 2015 eruption. Then, a volcanic eruption would induce depressurization of the reservoir, generating subsidence observed at the surface. This subsidence could trigger a reversal of the fault kinematics trend of the outward dipping ring fault from normal to reverse, with the slip initiating at the reservoir and propagating upward and not necessarily reaching the surface [Acocella, 2007] (Figure 3b). As a result, magma could propagate along the outward dipping ring fault and erupt inside the caldera (Figure 3c). This scenario helps to explain the two phases of eruptive activity observed at Wolf in 1982 and 2015. It also suggests that the two overlapping subsidence signals may be generated by a single deflating reservoir in combination with activity on a buried ring fault. Further depressurization of the reservoir would eventually lead to the ring faulting reaching the surface and even a caldera collapse with further localized deformation limited to the caldera floor, similar to recently observed activity at Bárðarbunga caldera in Iceland [Sigmundsson *et al.*, 2015; Gudmundsson *et al.*, 2016]. In conclusion, while the two subsidence patterns observed at Wolf can be well modeled using two reservoirs at different depths, consistent with inferences at Fernandina and Cerro Azul volcanoes, depressurization within a single reservoir in combination with activity on a buried ring fault might also be responsible for the observed deformation.

Acknowledgments

We thank Paul Segall (Stanford University), Charles Williams (GNS Science), and Geoff Wadge (University of Reading) for sharing the topography-correction codes. We also thank Renier Viltes (KAUST), Fabio Corbi (GFZ Potsdam), Eleonora Rivalta (GFZ Potsdam), Valerie Cayol (CNRS), Benjamin Bernard (IGEPN), and Patricio Ramon (IGEPN) for useful discussions. We used Generic Mapping Tools (GMT) to prepare Figure 1. The ALOS-2 data were provided by JAXA and the Sentinel-1A data by ESA/Copernicus. The research reported in this publication was supported by King Abdullah University of Science and Technology (KAUST).

References

- Acocella, V. (2007), Understanding caldera structure and development: An overview of analogue models compared to natural calderas, *Earth Sci. Rev.*, 85, 125–160.
- Acocella, V., R. Di Lorenzo, C. Newhall, and R. Scandone (2015), An overview of recent (1988 to 2014) caldera unrest: Knowledge and perspectives, *Rev. Geophys.*, 53, 896–955, doi:10.1002/2015RG000492.
- Amelung, F., S. Jónsson, H. Zebker, and P. Segall (2000), Widespread uplift and ‘trapdoor’ faulting on Galápagos volcanoes observed with radar interferometry, *Nature*, 407(6807), 993–996, doi:10.1038/35039604.
- Bagnardi, M., and F. Amelung (2012), Space-geodetic evidence for multiple magma reservoirs and subvolcanic lateral intrusions at Fernandina Volcano, Galápagos Islands, *J. Geophys. Res.*, 117, B10406, doi:10.1029/2012JB009465.
- Bagnardi, M., F. Amelung, and M. P. Poland (2013), A new model for the growth of basaltic shields based on deformation of Fernandina volcano, Galápagos Islands, *Earth Planet. Sci. Lett.*, 377, 358–366, doi:10.1016/j.epsl.2013.07.016.
- Baker, M. S. (2012), Investigating the dynamics of basaltic volcano magmatic systems using space geodesy, PhD dissertation, Univ. of Miami, Miami, Fla.
- Bathke, H., M. Nikkhoo, E. Holohan, and T. R. Walter (2015), Insights into the 3D architecture of an active caldera ring-fault at Tendürek volcano through modeling of geodetic data, *Earth Planet. Sci. Lett.*, 422, 157–168.
- Bernard, B., P. Ramon, H. Wright, A. Guevara, S. Hidalgo, D. Pacheco, D. Narvaez, and F. Vásconez (2015), Preliminary results on the 2015 eruption of Wolf volcano, Isabela island, Galápagos: Chronology, dispersion of the volcanic products, and insight into the eruptive dynamics, Abstract V31B-3022 presented at 2015 Fall Meeting, AGU, San Francisco, Calif., 14–18 Dec.
- Cayol, V., and F. H. Cornet (1998), Effects of topography on the interpretation of the deformation field of prominent volcanoes—Application to Etna, *Geophys. Res. Lett.*, 25, 1979–1982, doi:10.1029/98GL51512.
- Cervelli, P., M. H. Murray, P. Segall, Y. Aoki, and T. Kato (2001), Estimating source parameters from deformation data, with an application to the March 1997 earthquake swarm off the Izu Peninsula, Japan, *J. Geophys. Res.*, 106, 11,217–11,237, doi:10.1029/2000JB900399.
- Chadwick, W. W., Jr., and J. H. Dieterich (1995), Mechanical modeling of circumferential and radial dike intrusion on Galápagos volcanoes, *J. Volcanol. Geotherm. Res.*, 66, 37–52, doi:10.1016/0377-0273(94)00060-T.

- Chadwick, W. W., Jr., and K. A. Howard (1991), The pattern of circumferential and radial eruptive fissures on the volcanoes of Fernandina and Isabela islands, Galapagos, *Bull. Volcanol.*, 53(4), 259–275, doi:10.1007/BF00414523.
- Chadwick, W. W., Jr., S. Jónsson, D. J. Geist, M. Poland, D. J. Johnson, S. Batt, K. S. Harpp, and A. Ruiz (2011), The May 2005 eruption of Fernandina volcano, Galápagos: The first circumferential dike intrusion observed by GPS and InSAR, *Bull. Volcanol.*, 73(6), 679–697, doi:10.1007/s00445-010-0433-0.
- Chen, C. W., and H. A. Zebker (2001), Two-dimensional phase unwrapping with use of statistical models for cost functions in nonlinear optimization, *J. Opt. Soc. Am. A Opt. Image Sci. Vis.*, 18, 338–351, doi:10.1364/JOSAA.18.000338.
- Farr, T. G., et al. (2007), The shuttle radar topography mission, *Rev. Geophys.*, 45, RG2004, doi:10.1029/2005RG000183.
- Geist, D. J., T. R. Naumann, J. J. Standish, M. D. Kurz, K. S. Harpp, W. M. White, and D. J. Fornari (2005), Wolf Volcano, Galápagos Archipelago: Melting and magmatic evolution at the margins of a mantle plume, *J. Petrol.*, 46, 2197–2224, doi:10.1093/petrology/egi052.
- Geist, D. J., G. Bergantz, and W. W. Chadwick (2014) Galápagos magma chambers, in *The Galápagos: A Natural Laboratory for the Earth Sciences*, edited by K. S. Harpp et al., John Wiley, Hoboken, N. J., doi:10.1002/9781118852538.ch5.
- Global Volcanism Program (2015), Report on Wolf (Ecuador), in *Weekly Volcanic Activity Report*, edited by S. K. Sennert, 27 May–2 June 2015, Smithsonian Institution and US Geological Survey.
- González, P. J., M. Bagnardi, A. J. Hooper, Y. Larsen, P. Marinkovic, S. V. Samsonov, and T. J. Wright (2015), The 2014–2015 eruption of Fogo volcano: Geodetic modeling of Sentinel-1 TOPS interferometry, *Geophys. Res. Lett.*, 42, 9239–9246, doi:10.1002/2015GL066003.
- Grandin, R., M. Vallée, C. Satriano, R. Lacassin, Y. Klinger, M. Simoes, and L. Bollinger (2015), Rupture process of the $M_w = 7.9$ 2015 Gorkha earthquake (Nepal): Insights into Himalayan megathrust segmentation, *Geophys. Res. Lett.*, 42, 8373–8382, doi:10.1002/2015GL066044.
- Gudmundsson, M. T., et al. (2016), Gradual caldera collapse at Bárðarbunga volcano, Iceland, regulated by lateral magma outflow, *Science*, 353, aaf8988, doi:10.1126/science.aaf8988.
- Jónsson, S., H. Zebker, P. Cervelli, P. Segall, H. Garbeil, P. Mouginis-Mark, and S. Rowland (1999), A shallow-dipping dike fed the 1995 flank eruption at Fernandina Volcano, Galápagos, observed by satellite radar interferometry, *Geophys. Res. Lett.*, 26, 1077–1080, doi:10.1029/1999GL900108.
- Jónsson, S., H. Zebker, P. Segall, and F. Amelung (2002), Fault slip distribution of the 1999 $M_w 7.1$ Hector Mine, California, earthquake, estimated from satellite radar and GPS measurements, *Bull. Seismol. Soc. Am.*, 92, 1377–1389, doi:10.1785/0120000922.
- McBirney, A. R., and H. Williams (1969), Geology and petrology of the Galapagos Islands, *Geol. Soc. Am. Mem.*, 118, 1–197, doi:10.1130/MEM118-p1.
- Mogi, K. (1958), Relations between the eruptions of various volcanoes and the deformations of the ground surfaces around them, *Bull. Earthquake Res. Inst.*, 36, 99–134.
- Naumann, T., D. Geist, and M. Kurz (2002), Petrology and geochemistry of Volcan Cerro Azul: Petrologic diversity among the western Galápagos volcanoes, *J. Petrol.*, 43(5), 859–883.
- Okada, Y. (1985), Surface deformation due to shear and tensile faults in a half-space, *Bull. Seismol. Soc. Am.*, 75(4), 1135–1154.
- Rivalta, E., and P. Segall (2008), Magma compressibility and the missing source for some dike intrusions, *Geophys. Res. Lett.*, 35, L04306, doi:10.1029/2007GL032521.
- Schatz, H., and I. Schatz (1983), The eruption of the volcano Wolf (Albemarle, Galápagos islands, Ecuador) in 1982—Report of eye-witnesses [in German], *Ber. nat.-med. Verein Innsbruck*, 70, 17–28.
- Siebert, L., T. Simkin, and P. Kimberly (2010), *Volcanoes of the World*, Univ. of Calif. Press, Berkley.
- Sigmundsson, F., et al. (2015), Segmented lateral dyke growth in a rifting event at Bárðarbunga volcanic system, Iceland, *Nature*, 517, 191–195, doi:10.1038/nature14111.
- Simkin, T., and K. A. Howard (1970), Caldera collapse in the Galápagos Islands, 1968. The largest known collapse since 1912 followed a flank eruption and explosive volcanism within the caldera, *Science*, 169(3944), 429–437, doi:10.1126/science.169.3944.429.
- Williams, C. A., and G. Wadge (1998), The effects of topography on magma chamber deformation models: Application to Mt. Etna and radar interferometry, *Geophys. Res. Lett.*, 25, 1549–1552, doi:10.1029/98GL01136.
- Williams, C. A., and G. Wadge (2000), An accurate and efficient method for including the effects of topography in three-dimensional elastic models of ground deformation with applications to radar interferometry, *J. Geophys. Res.*, 105, 8103–8120, doi:10.1029/1999JB900307.
- Yang, X. M., P. M. Davis, and J. H. Dieterich (1988), Deformation from inflation of a dipping finite prolate spheroid in an elastic half-space as a model for volcanic stressing, *J. Geophys. Res.*, 93, 4249–4257, doi:10.1029/JB093iB05p04249.